THE TEMPERATURE DEPENDENCE OF THERMAL NEUTRON DIFFUSION LENGTH IN GRAPHITE

by

Frederick Faber Touchstone, Jr.

ADUATE SCHOOL
LIF. 93940

United States
Naval Postgraduate School

THESIS

THE TEMPERATURE DEPENDENCE OF THERMAL NEUTRON DIFFUSION LENGTH IN GRAPHITE

by

Frederick Faber Touchstone, Jr.

June 1970

This document has been approved for public release and sale; its distribution is unlimited.

134564

The Temperature Dependence of Thermal Neutron Diffusion Length in Graphite

by

Frederick Faber Touchstone, Jr.
Lieutenant Commander, United States Navy
B. S., United States Naval Academy, 1959

Submitted in partial fulfillment of the
requirements for the degree of

MASTER OF SCIENCE IN MECHANICAL ENGINEERING

from the

NAVAL POSTGRADUATE SCHOOL
June 1970

OSTGRADUATE SCHOOL
Y, CALIF. 93940

ABSTRACT

The existence of the two classes of thermal neutrons about the Bragg cut-off in a crystalline structure has been experimentally verified by the use of dysprosium-aluminum wire detector. The space dependent neutron flux in a 24x24x48 inch rectangular parallelopiped graphite pile, GLC grade HC and density 1.60 gm/cm^3, has been investigated at 295°K and 481°K. At each temperature a distinct "knuckle" or change of neutron distribution is readily apparent, although this degree of change decreases with increasing temperature because the neutron cross section below the Bragg cut-off increases with increasing temperature.

TABLE OF CONTENTS

ACKNOWLEDGEMENT

The author wishes to express his gratitude for the advice, encouragement and enthusiastic support given by Professor D. H. Nguyen throughout this investigation. His controlled guidance has been a pleasure and is greatly appreciated. A special thanks is due to Messrs. Ken Mothersell and Joe Beck for their ready willingness to assist in the construction phase of the experiment. The helpful and appropriate recommendations of Professor P. J. Marto are also acknowledged with thanks.

I. INTRODUCTION

A distinct characteristic of the neutron scattering cross section is known to exist in crystalline materials such as beryllium and carbon. The cross section above an energy level corresponding to the Bragg cut-off is relatively constant. However, below this energy level the cross section experiences a sharp drop, dividing the thermal neutrons into what may be called the cold neutron and thermal neutron groups. Additionally, within the cold neutron group, the cross section varies with the temperature of the material for any specific neutron energy. The existence of these groupings is graphically illustrated by the variation of diffusion length across the thermal neutron energy spectrum. The temperature dependence of the cold neutron group has been studied analytically and calculations made to determine the diffusion lengths in graphite at temperatures of 300°, 200°, 150°, and 100°K by Ahmed [2].

It was felt that experimental verification of this theoretical temperature dependence was in order. A thermal pile was constructed with provisions for raising the graphite temperature up to 650°K. Although Ahmed's calculations were based on below room temperature effects, the same dependency exists for the higher temperatures, as can be seen in Table 1 which includes values calculated by Trikha, et al. [21].

TABLE 1

TEMPERATURE (K°)	THERMAL GROUP L_T	COLD GROUP L_T	REFERENCE
100	225.21	141.75	21
150	92.10	45.00	2
200	62.80	43.10	2
300	56.75	24.25	21
300	58.30	25.00	2
373	59.85	20.38	21
523	65.17	15.96	21
609	67.73	14.49	21

II. THEORETICAL CONSIDERATIONS

A. CRYSTALLINE EFFECTS ON NEUTRON SCATTERING

Since the wavelengths of thermal neutrons are of the same order of magnitude (about 1.8 Å at room temperature) as the interatomic plane spacing for crystalline materials such as graphite, certain optical effects are observed. That is, all the interference effects associated with light and x-rays can be duplicated by the neutrons. It will be shown that there are energy regions where these optical effects may or may not be present. When they are present we have coherent scattering; that is, the kind of scattering that produces a wave capable of interfering with the incident neutron wave. In the absence of optical effects, the scattered wave does not interfere with the incident wave, resulting in "diffuse" scattering, called incoherent scattering.

The coherent scattering may be composed of both elastic and inelastic scattering. Incoherent scattering may also be either elastic or inelastic, broken down generally as follows: elastic incoherent may be due to the presence of different isotopes in the atomic lattice (which gives diffuse scattering), or due to the neutron spin relative to the nuclear spin; inelastic incoherent which is due to the energy exchange between a neutron and the medium's lattice vibrations, with the neutron absorbing one or more phonons (the lattice vibration quantum) of energy. This phonon energy may be from vibrations in any of the degrees of freedom.

The total cross section may then be written for the thermal region as:

$$\sigma_t = \sigma_a + \sigma_1 + \sigma_o + \sigma_{dis}$$

where σ_a is the capture cross section, σ_o is the coherent elastic scattering cross section, σ_{dis} is the incoherent elastic scattering cross section due to isotope presence or neutron/nucleii spin, and σ_1 is the inelastic incoherent and coherent scattering cross section due to phonon interchanges. In the thermal region, only the one phonon effect (neglecting the two or more phonon effects) makes any contribution to inelastic scattering [13].

In the case of graphite some of these terms may be eliminated. Since coherent inelastic scattering is low compared to the coherent elastic scattering it is generally neglected at energies below 1.0 ev. The capture cross section of graphite is small but proportional to 1/v. Since graphite is generally monoisotopic and has zero spin, the incoherent elastic scattering term drops out. Therefore there exists only

$$\sigma_t = \sigma_o + \sigma_a \qquad \text{(above Bragg cut-off)}$$

or

$$\sigma_t = \sigma_1 + \sigma_a \qquad \text{(below Bragg cut-off)}$$

In coherent scattering the mechanism by which waves capable of interfering with the incident neutron wave is governed by Bragg's law, written as

$$n\lambda = 2d \sin \theta$$

where n is the order of reflection, λ is the wavelength corresponding to the neutron energy, d is the plane spacing and θ is the angle between the direction of neutron propogation and the crystal plane. From this basic equation it is seen that there are many wavelengths (or energies) for which the coherent scattering mechanism is possible,

based on many different plane spacings. There is also a minimum energy corresponding to a maximum wavelength, $\lambda_{MAX} = 2d$, below which coherent scattering is not possible for any given plane spacing. For the largest plane spacing, the 002 plane in graphite, this minimum energy is called the Bragg cut-off, and no further coherent scattering can take place at lower energies. For graphite, the average room temperature crystalline 002 plane spacing d is 3.3538 Å (Ångstroms). Using the deBoglie relation

$$\lambda = \frac{h}{p} = \frac{h}{mv}$$

or

$$v = \frac{h}{\lambda m}$$

where h is Planck's constant, p is momentum, m is the neutron mass and v is the neutron velocity, the energy of this Bragg cut-off can be determined.

$$KE = \frac{1}{2} mv^2$$

$$KE = \frac{1}{2m} \left(\frac{h}{\lambda} \right)^2$$

$$KE_{MIN} = \frac{1}{2m} \left(\frac{h}{2d} \right)^2$$

Substitution of the values for neutron mass, Planck's constant and plane spacing yields a Bragg cut-off energy of 0.001823 ev. Thus, for all energies above this value (a region occupied by neutrons of the thermal group) coherent elastic scattering is the dominant factor, while at lower energies, for neutrons of the cold group, incoherent inelastic scattering alone dominates.

Although the frequency of the lattice vibrations is largely independent of temperature, the amplitude increases with increasing

temperature [8]. This increased amplitude results in increased lattice energy and therefore larger one phonon energies, giving greater incoherent inelastic scattering. Additionally it can be shown [10] that the incoherent inelastic scattering is proportional to the wavelength, or follows the "1/v law", and that it increases rapidly with temperature (about linear by observation, as opposed to the T^2 behavior predicted by the usual Debye frequency spectrum). Capture cross section, however, is temperature independent for all thermal energies. Figures 1 and 2 show the coherent and incoherent scattering cross section regions. The combined effects of these graphite scattering cross sections, along with its capture cross section is seen in Figure 3.

B. DIFFUSION OF NEUTRONS IN A CRYSTALLINE MODERATOR

The diffusion length can be defined by

$$L^2 = \frac{1}{3} \cdot \lambda_{tr} \cdot \frac{1}{\Sigma_a}$$

$$L^2 = \frac{1}{3} \cdot \frac{1}{n\sigma_{tr}} \cdot \frac{1}{\Sigma_a}$$

where λ_{tr} is the transport mean free path, Σ_a is the macroscopic capture cross section, n is the number of atoms per unit volume and σ_{tr} is the transport cross section. In the thermal neutron group region, above the Bragg cut-off, the value of σ_{tr} will be largely that of the elastic coherent scattering cross section, σ_o. It is generally assumed to be given, away from the immediate vicinity of the Bragg cut-off, by its asymptotic value $\sigma_s (1 - \frac{2}{3A})$ [1], where σ_s

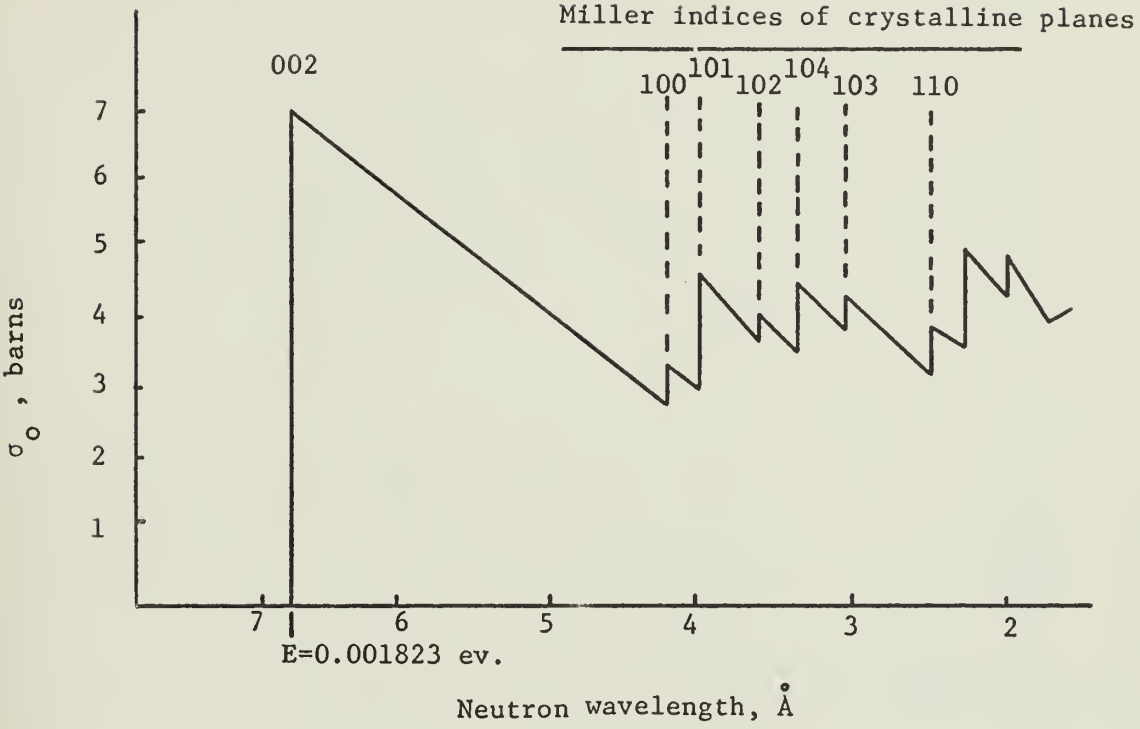

Fig. 1

Elastic (Bragg) coherent scattering cross section of graphite, [6]

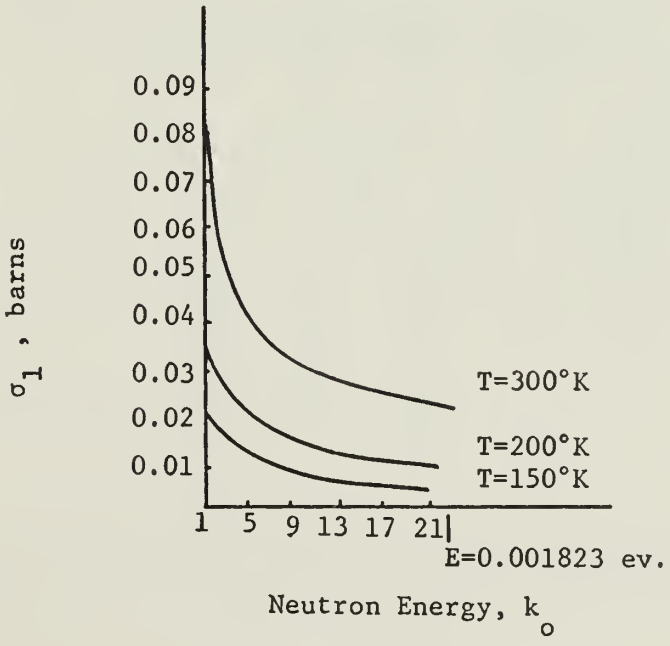

Fig. 2

Inelastic incoherent scattering cross section of graphite (k_o is Bolzmann's constant), [1]

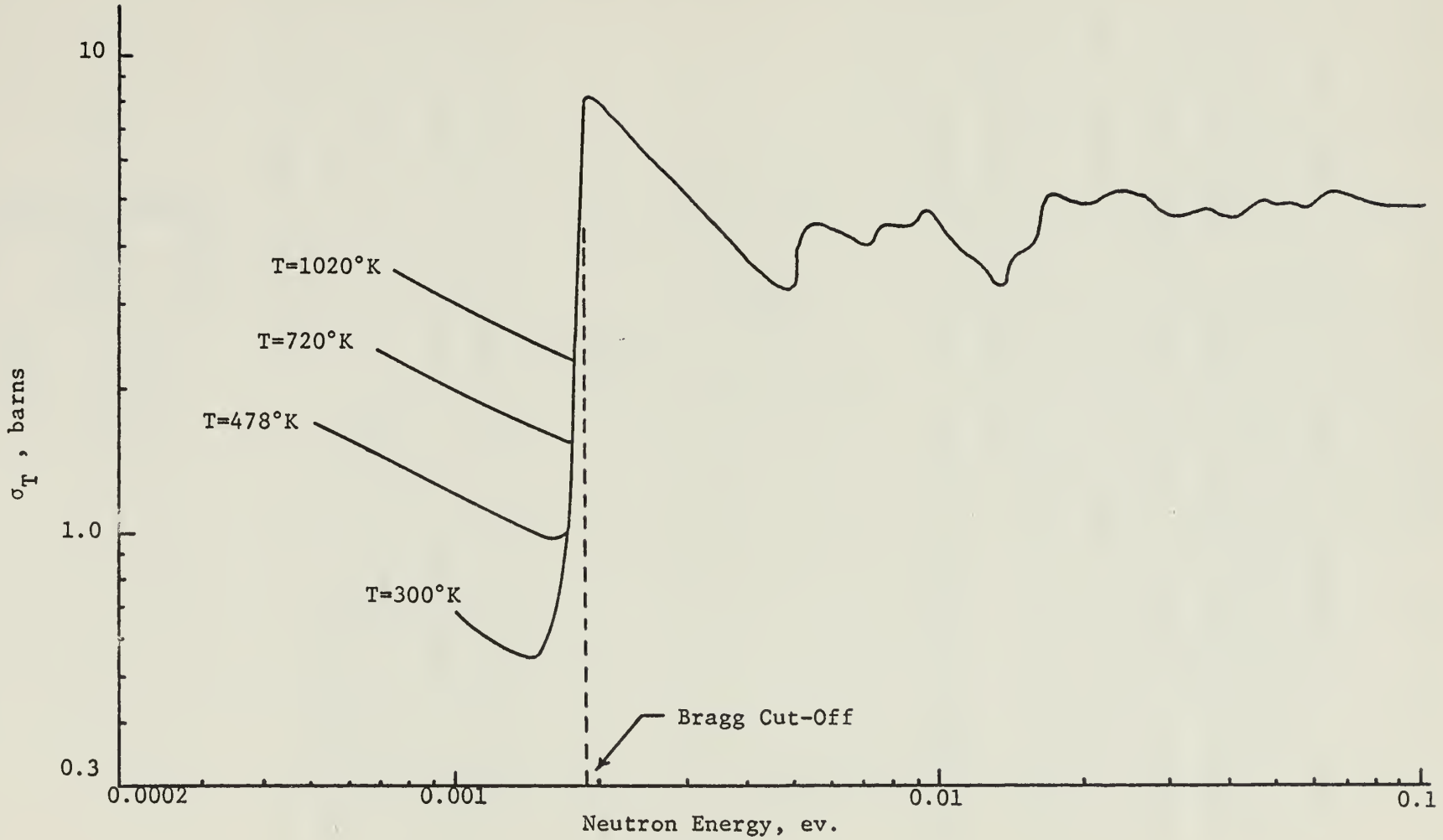

Fig. 3
Total Neutron Cross Section of Graphite, [11]

is the microscopic (coherent elastic) scattering cross section and A is the atomic mass number. The temperature dependence of this cross section is very small. In the cold neutron group region σ_{tr} can be taken to be equal to σ_1, the incoherent inelastic cross section due to the one phonon effect. As pointed out above, and shown in Figure 2, this cross section increases with temperature. Therefore, the diffusion length should decrease with increase of temperature for energies in the cold neutron group, while remaining essentially constant with temperature for energies above the Bragg cut-off.

The time independent, isotropic diffusion equation for thermal flux can be written as

$$\nabla^2\phi(\bar{r}) - \frac{1}{L_T^2}\phi(\bar{r}) = 0 \qquad (1)$$

where

$$L_T = \left(\frac{\bar{D}}{\bar{\Sigma}_a}\right)^{1/2}$$

and where $\bar{D}$ and $\bar{\Sigma}_a$ are the average values in the thermal region for diffusion coefficient and macroscopic capture cross section, respectively. Equation (1) can be written for two regions of energy, the cold and thermal groups, with the values of $\bar{D}$ and $\bar{\Sigma}_a$ being determined over the appropriate energy range.

$$\bar{D}_1 = \frac{\int_{0.0018}^{E_T\sim 1ev} D(E)\,\phi(E)\,dE}{\int_{0.0018}^{E_T\sim 1ev} \phi(E)\,dE}$$

$$\bar{D}_2 = \frac{\int_0^{0.0018} D(E)\,\phi(E)\,dE}{\int_0^{0.0018} \phi(E)\,dE}$$

$$\bar{\Sigma}_{a1} = \frac{\int_{0.0018}^{E_T\text{-lev}} \Sigma_a(E)\,\phi(E)\,dE}{\int_{0.0018}^{E_T\text{-lev}} \phi(E)\,dE}$$

$$\bar{\Sigma}_{a2} = \frac{\int_0^{0.0018} \Sigma_a(E)\,\phi(E)\,dE}{\int_0^{0.0018} \phi(E)\,dE}$$

Thus,

$$\nabla^2\phi_1(\bar{r}) - \frac{1}{L_{T1}^2}\,\phi_1(\bar{r}) = 0 \qquad (1\text{-a})$$

and

$$\nabla^2\phi_2(\bar{r}) - \frac{1}{L_{T2}^2}\,\phi_2(\bar{r}) = 0 \qquad (1\text{-b})$$

where the subscripts 1 and 2 refer to the thermal neutron group and cold neutron group, respectively. With the source placed at the center of the base of a rectangular parallelopiped, $\phi(x,y,0)$ will be symmetric about the origin and the flux will be an even function of

both x and y throughout the pile. The solution to equations (1-a) and (1-b) has the same form. It can be shown that (dropping subscripts for simplicity) the solution is [15]

$$\phi(x,y,z) = \sum_{\substack{m,n \\ \text{odd}}} A_{mn} \cdot \sinh \gamma_{mn}(c-z) \cdot \cos \frac{m\pi x}{a} \cdot \cos \frac{n\pi y}{a} \qquad (2)$$

where

$$A_{mn} = \frac{4}{a^2 \sinh(\gamma_{mn} c)} \int_{-a/2}^{a/2} \int_{-a/2}^{a/2} \phi_T(x,y,0) \cos\frac{m\pi x}{a} \cos\frac{n\pi y}{a} \, dx \, dy$$

γ_{mn} is the relaxation length and is expressed as

$$\gamma_{mn}^2 = \frac{1}{L_T^2} + \left(\frac{m\pi}{a}\right)^2 + \left(\frac{n\pi}{a}\right)^2 \qquad (3)$$

c is the vertical extrapolated height of the pile.

a is the extrapolated horizontal dimension of the pile.

x,y,z are the co-ordinates from an origin at the bottom center of the pile.

Since measurements are made along the centerline of the pile where $x = y = 0$, equation (2) simplifies further to

$$\phi(0,0,z) = \sum_{\substack{m,n \\ \text{odd}}} A_{mn} \sinh(c-z)$$

or in exponential terms

$$\phi(0,0,z) = \frac{1}{2} \sum_{\substack{m,n \\ \text{odd}}} A_{mn} \left[e^{\gamma_{mn}(c-z)} - e^{-\gamma_{mn}(c-z)} \right] \qquad (4)$$

In a pile measurement the height c is much larger than the diffusion length so that in areas not too near the top, the term $\gamma_{mn}(c-z)$ becomes very large and the second term of equation (4) can be neglected. Then

$$\phi(0,0,z) = \frac{1}{2} \sum_{\substack{m,n \\ \text{odd}}} A_{mn} e^{\gamma_{mn} c} \cdot e^{-\gamma_{mn} z}$$

and by defining

$$C_{mn} = \frac{1}{2} \sum_{\substack{m,n \\ \text{odd}}} A_{mn} e^{\gamma_{mn} c}$$

$$\phi(0,0,z) = \sum_{\substack{m,n \\ \text{odd}}} C_{mn} e^{-\gamma_{mn} z} \tag{5}$$

$$\phi(0,0,z) = C_{11} e^{-\gamma_{11} z} + C_{13} e^{-\gamma_{13} z} + C_{31} e^{-\gamma_{31} z} + \ldots$$

Hughes [10] points out that as the distance from the source increases, the effect of the higher harmonics (γ_{13}, γ_{31}, et cetera) becomes negligible and that the neutron distribution is practically exponential beyond that distance. Also Kaiser and Kimel [12] have computed the relative contributions of the γ_{13} harmonic for a graphite pile as a function of distance from the source. They show γ_{13} to be approximately one-tenth the contribution of γ_{11} for a constant thermal source at a distance of 20 inches from the source.

Therefore by concentrating on the mid-axis range — from 35 cm to 80 cm — it is possible to neglect the higher harmonics and end effects so that

$$\phi(0,0,z) \approx C_{11} e^{-\gamma_{11} z}$$

or

$$\ln \phi = \ln C_{11} - \gamma_{11} z \qquad (6)$$

which is a simple, one degree polynomial equation of intercept $\ln C_{11}$ and slope $-\gamma_{11}$ on a $\ln \phi$ versus z plot. The form of this equation is valid for both thermal and cold neutron groups.

Least squares polynomial approximations over the region of validity for each group results in the determination of their respective γ_{11}. Since the relaxation length is a function of L_T and it has been shown that diffusion length for an infinite medium changes across the Bragg cut-off, it follows that the values of γ_{11}, or the slopes of the plot, should change also. This will occur at some point in the pile at which the cold neutrons have been filtered through in appreciable number.

Similarly the degree of slope in each instance will change with a temperature change. The greater degree of change will be present in the cold group region neutrons, that is, the region where the number of cold neutrons is appreciable. Since, as was pointed out, the incoherent inelastic scattering in this region is highly temperature dependent, an increase in temperature will result in increased scattering cross section and reduced diffusion length. A lower diffusion length is associated with an increased slope γ_{11} (refer to equation (3)). In the thermal neutron group, the transport mean free path has been found by Lloyd, et al. [16] to decrease slightly with temperature. Therefore with higher temperatures the diffusion length would increase and the slope γ_{11} would decrease. The overall effect

of high temperature will then be to increase the slope of the first part of the neutron distribution curve (before the "knuckle") and decrease the slope of the second (or cold neutron) part of the curve (beyond the "knuckle"). At a sufficiently high temperature the "knuckle" will vanish and a single slope will exist for the entire thermal range. According to cross section data from Ref. [11], this temperature should be higher than 1020°K.

III. PROJECT DESCRIPTION

It was proposed to verify experimentally: first, that the thermal neutron diffusion lengths above and below the Bragg cut-off energy did, in fact, differ; and second, that this difference decreased as temperature increased. The neutron flux plot should change from a distinct "knuckle" at the location where the number of cold neutrons becomes appreciable to a single, continuous line at very high temperatures.

IV. TEST APPARATUS

A. DESCRIPTION

1. General

It was originally planned to utilize the AGN 201 reactor at the Naval Postgraduate School reactor facility as the neutron source for this experiment. However, the physical construction of the reactor did not provide for removal of any segments of its shielding. It would have been necessary to construct the graphite pile outside the reactor — a distance of some 7.5 feet from the reactor core center — over one of the access holes or the "glory hole". It would be necessary for the reactor to be operated at its maximum power of 1000 watts (which could only be sustained for about ten minutes) in order for sufficient neutron flux to be obtained in this manner. This short time period was quite insufficient for any flux measurement in the proposed sigma pile.

Therefore it was decided to utilize three Plutonium-Beryllium neutron sources: two sources of 1.8×10^6 n/sec each, and one source of 5.4×10^6 n/sec. These were the only other continuous neutron sources available. The most probable energy of these neutron sources is about 4.0 Mev [3], so it would be necessary to provide for additional slowing down time.

2. Graphite Pile

The graphite pile consisted of a rectangular parallelopiped constructed of one hundred twenty eight (128) graphite bricks, each one 3 x 6 x 12 inches. The base was two feet square and the height was four feet. Figure 4 gives a cross sectional view of the pile's general arrangement. Great Lakes Carbon Corporation, Grade HC, graphite of density 1.60 gm/cm^3 was utilized. The use of this relatively impure

graphite as opposed to AGOT nuclear graphite was considered acceptable in view of the experiment's primary aim in investigating temperature dependence rather than absolute values. A three sixteenth inch vertical hole was drilled down the entire four foot centerline of the pile to provide for the detecting wire used.

3. Heating and Insulation

Heating of this pile was achieved by twenty calrod strip heaters of 21.5 inches heating length, 1.5 inches width and 3/8 inch thickness arranged about all four sides, the top and bottom. Close fit grooves, 1.5 by 3/8 inch, were cut in the graphite bricks, three inches in from the side faces and six inches in from the top and bottom, prior to assembly to accomodate these heaters. The grooves were a full 24 inches long, the same size as the pile, in order to provide for thermal expansion of the heater elements. Figure 5 shows the external arrangement of graphite bricks and groove openings. Each heater was rated for 750 watts at 220 volts, providing for 15 kVA of heating capacity. Heaters were regulated in pairs by ten variacs which provided excellent control of heat throughout the pile. Figure 6 shows control table arrangement with the variacs and thermocouple readout instruments.

The design of insulation was entirely dictated by the availability of insulating materials within the campus. Fire brick was used as the base insulation since it was strong enough in compression to support the 1590 pound weight of the graphite and also had excellent insulating properties. A sheet of three sixteenth inch asbestos cement board separated the fire brick from the half inch steel plate which acted as a table to support the pile over the neutron source. Both the steel plate and fire brick had a three inch hole at the pile centerline

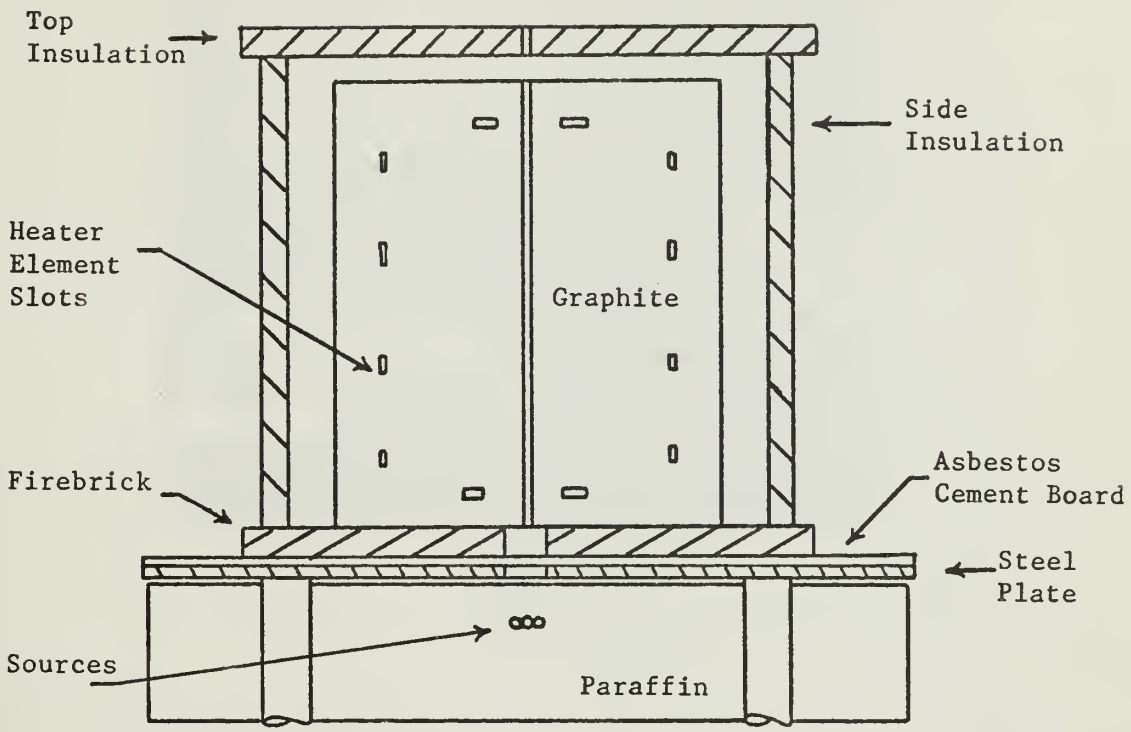

Fig. 4

Cross Section of Pile General Arrangement

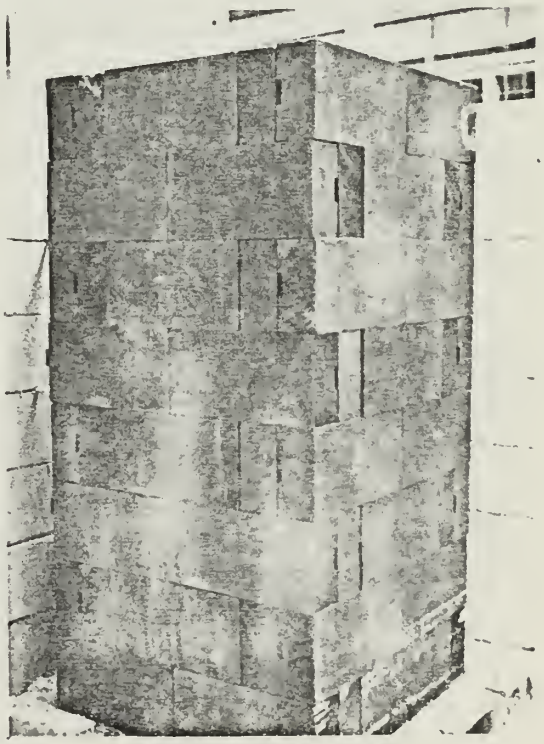

Fig. 5

External Arrangement
of
Graphite Bricks

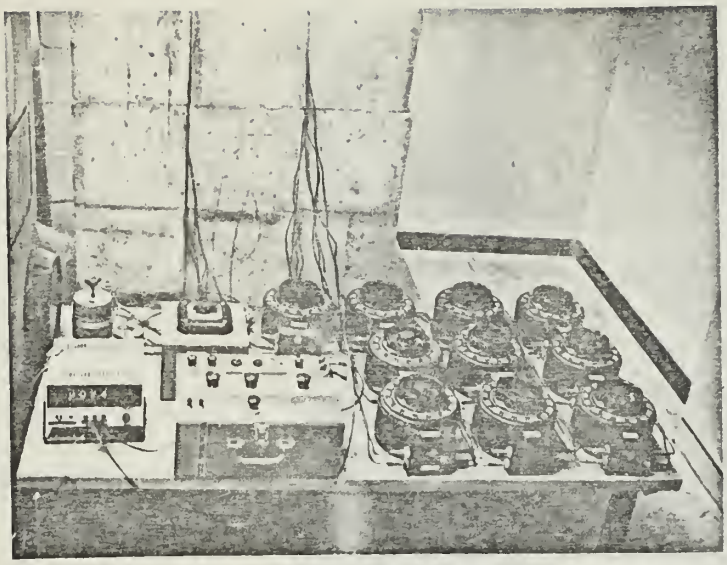

Fig. 6

Control Table Arrangement

to reduce neutron scattering in that immediate vicinity. Two types of insulating block, using readily available material, were installed about the four sides at a distance of about three inches from the pile. A two inch layer of glass wool insulation attached to the underside of a plywood board encased the top of the insulating walls, also with an air gap, thus completely insulating the graphite pile. The air gaps were provided in an attempt to reduce to a minimum the backscatter that may have occurred from the insulating material, thus making possible the use of the simplified diffusion equation given as equation (1). Figure 7 shows the lower corner of the graphite pile to illustrate the base and side insulation, as well as the heating element connections.

4. Temperature Determination

Ten copper-constantan miniature thermocouples were arranged in groups of five each in planes that were twelve and thirty six inches respectively from the base. In each plane one thermocouple was at the centerline of the pile and the other four were three inches from the

Fig. 7
Lower Corner
of
Graphite Pile

centerline. The closest any thermocouple was to any heating element was 6.72 inches and the most distant was 7.51 inches. Due to symmetry of all heating element locations, the thermocouples were equally affected by the aggregate heaters. This arrangement of thermocouples allowed determination of temperature uniformity throughout the volume of graphite for which the diffusion length was measured. A multiple switch was utilized to give a common reference junction of 0°C to all thermocouple readings. A plain water ice bath in a thermos jug served as the reference junction. A digital potentiometer provided the voltage readout continuously to within a tenth of a millivolt. A galvanometer-type millivolt potentiometer with accuracy to $\pm$1.0 microvolt was utilized for final voltage determination after the system had settled out and for accurate temperature determination during irradiation runs.

It was recognized that copper was probably the worst possible constituent to use in a nuclear radiation experiment for temperature determination. As pointed out by Ross [18], the percentage change of resistivity with temperature in a neutron flux can be expressed by:

$$\% \frac{\Delta\rho}{\rho_o} = 220 \times 10^{-22} \phi t$$

compared to that for constantan:

$$\% \frac{\Delta\rho}{\rho_o} = 4.7 \times 10^{-22} \phi t$$

where $\Delta\rho$ is the change of resistivity, ρ_o is the original resistivity, ϕ is the neutron flux and t is the time in the neutron flux in seconds. However, the low neutron flux available for this experiment and the relatively short exposure times permitted the neglect of this shortcoming. As with the decision to use plain water versus pure water in the ice bath, the accuracy of termperature determination was deemed sufficient to within five degrees centigrade.

5. Neutron Source

The three Plutonium-Beryllium (Pu-Be) sources were grouped together in a horizontal plane beneath the base of the pile directly under the centerline axis. A single one and three quarter inch layer of paraffin was placed above the sources to aid in slowing down the high energy neutrons before they entered the graphite. Numerous arrangements of source height position and thickness of paraffin were tried before the above set up was decided upon. It was found that the paraffin not only slowed down but absorbed the neutrons so much that the flux was reduced to an unacceptable level. Therefore only one

layer was utilized. This layer and the source under it were placed as close to the base as possible since it was also postulated that the air gaps present, and the different medium through which the neutrons travelled before reaching the graphite all contributed to the low flux within the graphite. Since these neutrons were of a higher energy than normally encountered in experiments of this nature, it was thought that they would require a much larger amount of moderating material to reach thermal energies. However a quick calculation of the number of collisions required to achieve this energy in hydrogenous moderators (assuming the same logarithmic decrement as water) showed as follows:

4.0 Mev neutrons: $n = \frac{1}{\xi} \ln \frac{E_o}{E} = \frac{1}{0.92} \ln \frac{4 \times 10^6}{1}$

$n = 16.5$ collisions to reach 1.0 ev

2.0 Mev neutrons: $n = \frac{1}{\xi} \ln \frac{E_o}{E} = \frac{1}{0.92} \ln \frac{2 \times 10^6}{1}$

$n = 15.78$ collisions to reach 1.0 ev

With a transport mean free path of 0.395 cm for paraffin [20] (the average distance between collisions), this indicated that only an additional 0.284 cm would be required to achieve thermal energies.

Blocks of paraffin surrounded the sides of the source to a thickness of two and one half feet and were arranged outside the graphite insulation to protect personnel in the area. The neutron leakage through this arrangement was surveyed and found negligible.

6. Neutron Detection

It was originally planned that a BF_3 neutron detector, in conjunction with a multi-channel analyzer, would be used to take an

integrated count at each axial position. Investigation showed that this detector would withstand temperatures only as high as 150°C. Similar restrictions were found to exist for solid state detectors as well as indium and cadmium, which melt at 156°C and 320.9°C, respectively. A few solid state detectors were available commercially but to achieve the sensitivity required for the low flux measurements in this experiment, their size was much too large. Gold foils, though commonly used for high temperature measurements offered such a long half-life as to be not feasible from irradiating time considerations. A detecting wire of 11.4 per cent dysprosium-aluminum alloy was finally chosen, based on its high melting temperature and convenient (2.35 hour) half-life. A purity of 99.94 per cent was certified by the manufacturer and impurities listed by name indicated no need for their consideration or possible effect on the dysprosium capture cross section; although this factor was taken into account in computing the total number of dysprosium atoms, described in Appendix A. An average atomic weight of 162.5 was determined based on the percentage of the various isotopes to be found in natural dysprosium. A value of 930.0 barns was used as the capture cross section, as recommended [7]. This coincides with the value obtained by weighting the cross sections of each isotope in accordance with their abundance in natural Dy, Dysprosium has a small response to epithermal neutrons [14,19]. The maximum epithermal contribution to the total dysprosium activity has been found to be less than two per cent [4]. Therefore the activity determined with this dysprosium wire was considered to be completely due to thermal flux. The detecting wire was positioned in the three sixteenth inch axial hole along the entire pile height during irradiation. A thin glass tube held the wire segments in position.

On initial irradiation tests the reactor facility counting equipment was utilized. This consisted of a thallium-activated sodium iodide crystal and photo-multiplier, a pulse height analyzer for total decay count determination, and a multi-channel analyzer for energy spectrum readout and analysis (as a side benefit and not directly connected with the object of the experiment). It was later found to be more practical to utilize the counting equipment of the laboratory adjacent to the experimental room. This involved a Geiger-Mueller tube operating with 1400 volt D.C. bias, and pulse height analyzer. The efficiency of the G.M. counting system for beta counting was determined to be approximately twenty-seven per cent, while that of the photo-crystal for gamma counting in the reactor facility was about twenty-nine per cent, so that no appreciable advantage could be gained by the latter's utilization other than familiarization with another piece of equipment.

B. OPERATION

Test runs were made at room temperature and at an elevated temperature of 481°K. The following operational procedures were followed in both cases except for temperature control.

Two main fifty ampere circuit breakers were turned on to provide a maximum of 6.8 amperes to each of ten variacs, which in turn provided 3.4 amperes to each of two heating elements. The variacs were connected such that five of them controlled the bottom ten heaters and five of them controlled the top ten heaters. Similarly each variac controlled the same two elements at a particular height so that even control of temperature could be achieved. All variacs were gradually increased to slowly raise the pile temperature to the desired level with the minimum

amount of "hunting". It was found that the temperatures at each thermocouple grouping were consistently even, within 2°C of each other. It was thus only necessary to adjust the top with the bottom groupings. This was a fairly easy task and temperature variations between any of the ten thermocouples amounted to a maximum of plus or minus 4.56°C. The final test temperature value is the mean of the ten readings, which are about constant, over the entire irradiation time span.

Once the specified temperature equilibrium was achieved, the three sources were placed in position under the graphite pile. In order to utilize the counting equipment and obtain the activity at a particular location it was necessary to cut the detecting wire into one inch segments. Due to the cost of the wire, segments had to be used over again, necessitating a requirement for being able to insert and remove segments to a known axial position. This was achieved through the use of a thin glass tubing the length of the graphite pile, into which the wire segments could be inserted. The bottom of the tube was sealed with a glue to prevent segments from dropping out. A maximum of eight segments could safely be inserted in the glass tubing without the glass fracturing. Since 48 data points were being taken this meant at least six irradiation periods for each test run. An average irradiation period of eight hours provided ninety per cent of full saturation. After irradiation the tube was withdrawn, the bottom two elements removed by snapping off the glass tubing at that point, adding a drop more glue to the new bottom of the tube, and reinserting the tube, maintaining segment axial position, to continue the irradiation procedure while the two elements removed were being counted for decay activity. Due to the low flux, long (thirty minute) counting times per

segment were required. Since even during the short time of absence from the flux for segment removal a significant decay occurred in the remaining segments, it was necessary to derive the iterative formula for the activity at each subsequent removal time as described in Appendix A.

Upon removal of the two segments a period of seven minutes was allowed to elapse in order to reduce the 75 second half-life of Dy^{165} to a negligible effect. During this time, ten minute background counts were obtained, to be averaged together and applied to the segment total activity count. During the initial stages of the experiment, using the reactor facility equipment, the energy spectrum of the decaying wire segment was determined from the multi-channel analyzer. Although the decay rates were very small, a typical dysprosium gamma ray spectrum was obtained with no indication of any other material being present, validating the stated composition of dysprosium and aluminum. Throughout the entire experimental testing, accurate determination and recording of time was maintained.

The individual wire segments were used in the same axial position for both runs to insure consistency in obtaining data.

C. FAILURES AND MALFUNCTIONS

The scope of the original project definition had to be curtailed drastically for a number of reasons, some already stated:

1. Detector Restrictions

The high temperatures sought to be achieved drastically restricted the choice of detectors available. The state of the art in neutron detectors, especially in high temperature ranges, is geared toward very high flux ranges as found in reactors. This required the use of a dysprosium wire which, while offering negligible self-shadowing

and being sensitive mostly to thermal neutrons, also was too small to make up the adverse effects of low flux. Since the wire was very expensive it was necessary to find some method of re-using the segments after they had been previously used.

A tubing arrangement was decided upon as offering the simplest method of positioning and handling the segments. Glass tubing was readily available but, due to its brittleness, there was a high probability of tube fracture and subsequent loss inside the pile. This method was to be used only as a last resort. Three different metal tubes of various sizes were tried. However, in each case the segments bound up inside the tubing, necessitating the cutting of the tubes to remove the segments. It was finally resolved that the wire was too soft to be stacked inside a tube or pushed through it by a rod. The slightest buckle produced a jamming against the tube walls, inducing further binding. Therefore the glass tubing was resorted to, as described in the operating procedures, with utmost caution being taken to avoid fracture inside the pile.

2. Heat Considerations

The Pu-Be source provides neutrons from the alpha particles (given off by plutonium decay) interacting with the beryllium to give off neutrons (Be(α,n) reaction). There is the possibility that some alpha particles would pick up electrons to become helium gas before an interaction with beryllium could occur. Thus it was decided to keep the sources at room temperature to prevent a possible rupture of the source cladding due to gaseous expansion, despite assurances from the manufacturer that no hazard existed. Coincidentally, by maintaining the sources at one temperature for all tests a more realistic comparison

of data would be possible since the source spectrum could be a function of temperature.

This tremendously complicated the construction of the experimental set-up. With the existing insulation installed below the base, a design was provided to have an air channel over the source and its moderating paraffin layer. A small blower motor was to have been installed to force cooling air through the channel and out an exhaust ducting. However, when it became apparent that the flux level was going to be too low, it was necessary to do away with the air channel and move the paraffin and source as close to the base as possible. A remote reading bourdon temperature gage was installed between paraffin layers in order to keep the source temperature under constant surveillance.

During heating operations the temperature variation between all measuring thermocouples was easily kept within the limits desired. It was found however that over a period of time the steel plate began to heat up to such a degree as to affect the paraffin. This was traced to the three inch square hole in the firebrick below the graphite. Although there was also a hole in the steel plate at that location, the single sheet of asbestos sheet cement did not offer long term heat insulation properties and conducted the heat throughout the steel plate underneath. By filling this hole in the firebrick arrangement with plastic refractory and a small sheet of insulating block, it was possible to eliminate the problem of the hot steel plate. As an additional measure, some of the surrounding paraffin in close proximity to the steel plate was removed, while leaving the paraffin around the source. This provided a cavern effect around the center column of

paraffin and source (which remained in place, close to the graphite base). The air blower originally planned for was then installed to circulate air through this cavern and around the source, rather than over it as was originally planned. This proved quite satisfactory and no further heat problems were encountered.

V. DATA ANALYSIS AND RESULTS

A. DATA REDUCTION

A total of forty eight data points were collected for the room temperature test. After the break in the slope was located from this run, only the center twenty two positions were investigated for the high temperature test. The saturation activity and corresponding thermal flux was computed as shown in Appendix A. The uncertainties are described in Appendix B.

The natural log of the flux was then plotted versus the height in order to determine where the break in the slope might occur. As noted in the theory, only the center portion of the pile was to be investigated. A general trend or indication of where the fundamental slope γ_{11} became predominant was also of interest in choosing points for the least squares approximation, however, so all points were initially plotted. These are shown in Figure 8. Once the apparent Bragg cut-off break point was fixed upon, the points making up the two slopes were submitted to separate least squares polynomial approximations to obtain a mean value of slope and a standard deviation. By applying Chevenet's criterion [9] for rejecting an experimental reading, certain points were eliminated for each slope. The remaining data points, those within the criterion, were submitted to a final least squares fit. The slopes obtained in this manner were entered in equation (3) to determine the diffusion lengths. The slopes γ_{11} and diffusion lengths L_T are shown in Table 2 for both temperature conditions.

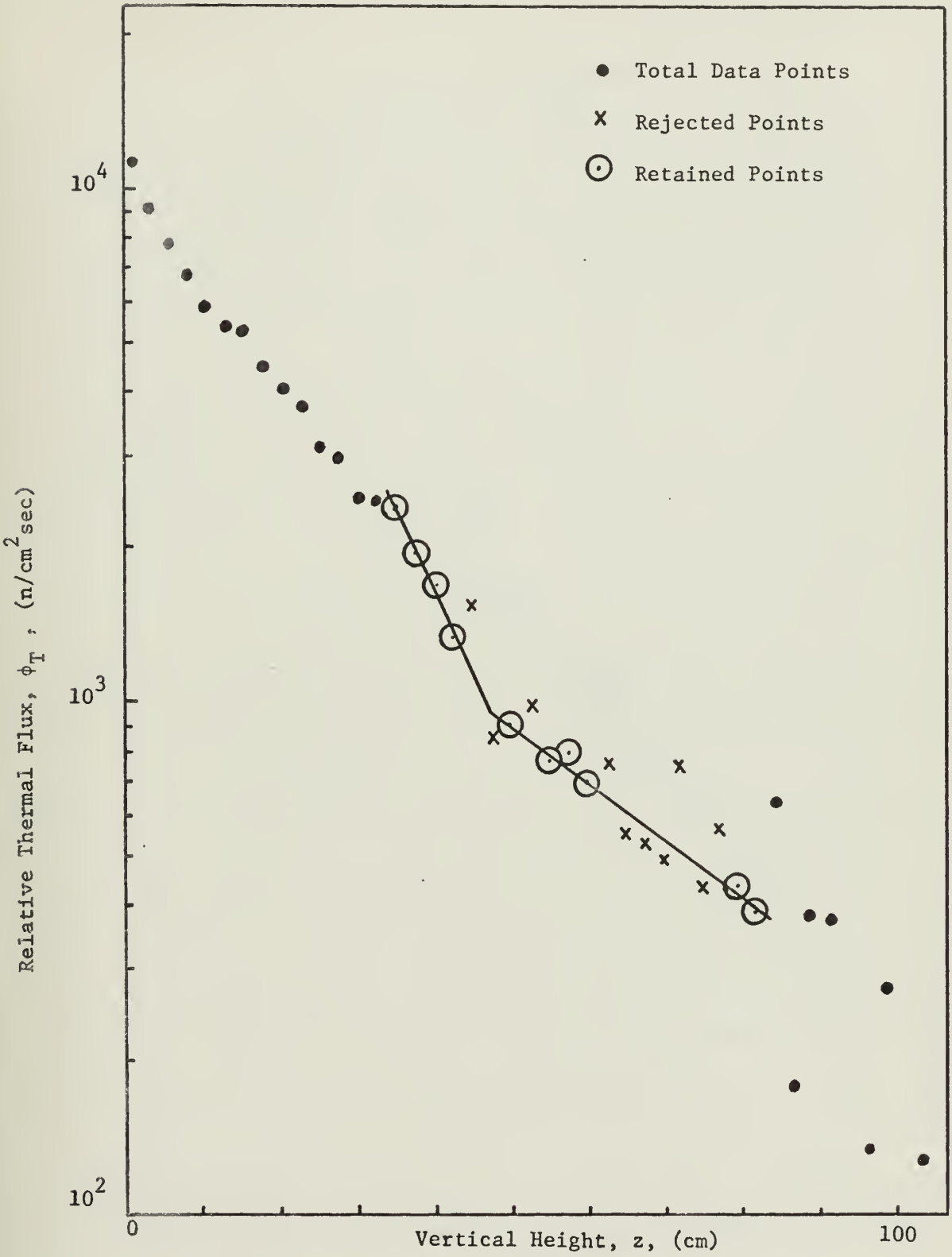

Fig. 8

Thermal Flux versus Height for Graphite Temperature of 295°K

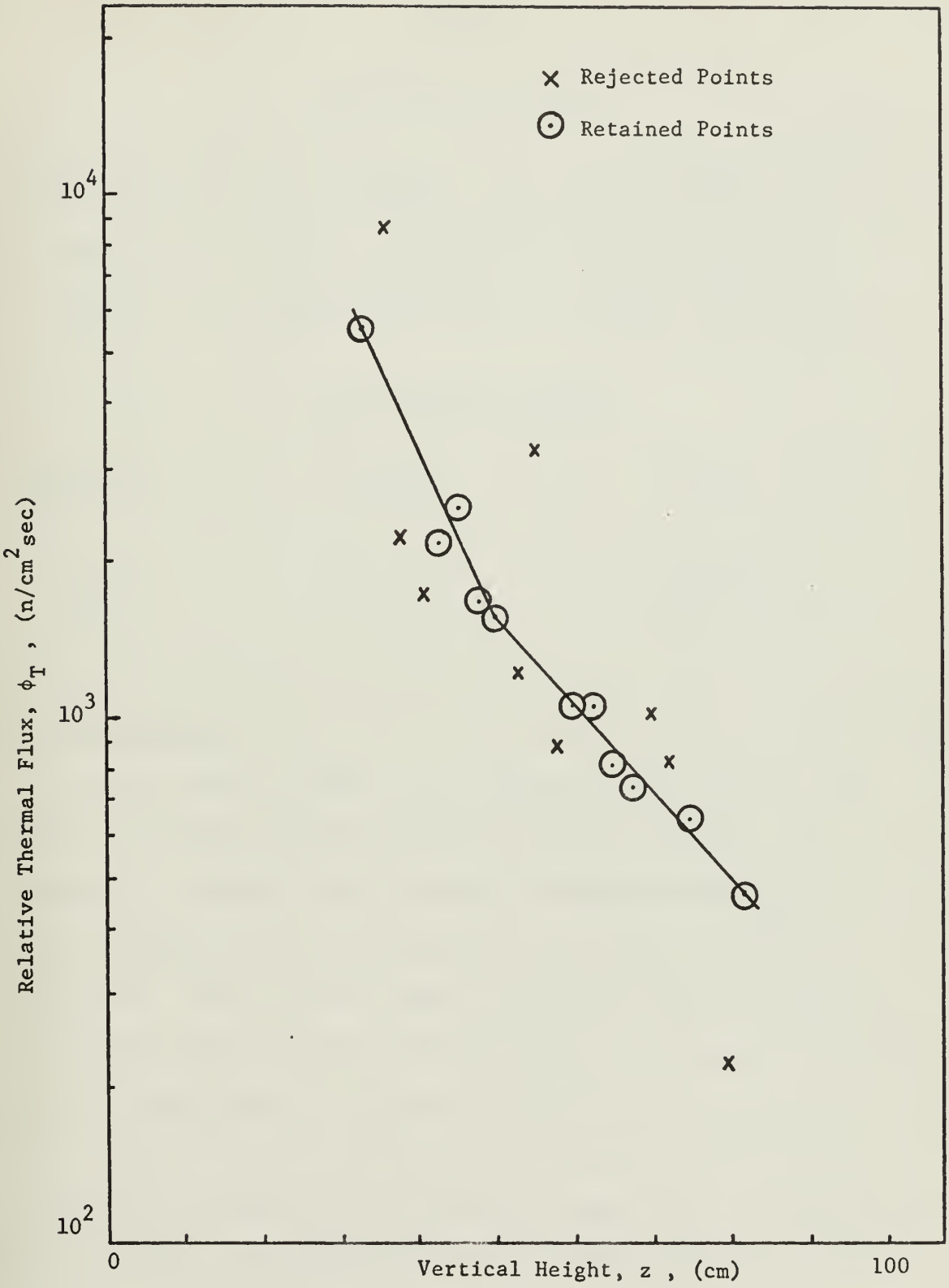

Fig. 9

Thermal Flux versus Height for Graphite Temperature of 481°K

TABLE 2

γ_{11}(relaxation length)

Temperature	Thermal	Cold
295°K	0.077 ± 0.013 cm^{-1}	0.026 ± 0.004 cm^{-1}
481°K	0.074 ± 0.024 cm^{-1}	0.037 ± 0.008 cm^{-1}

L_T (diffusion length)

Temperature	Thermal	Cold
295°K	32.72 cm	Imaginary
481°K	45.49 cm	Imaginary

B. FINAL RESULTS

As can be seen from Table 2 the diffusion lengths are much lower than those normally found for thermal neutrons in graphite. For instance S. K. Trikha, et al. [21] have calculated thermal group diffusion lengths of 56.75 cm and 65.17 cm for 300°K and 523°K, respectively. Also they have found a cold group diffusion length of 24.25 cm and 15.96 cm for the same temperatures. In the present case the thermal group diffusion lengths are much lower. For the cold group, L_T becomes imaginary. That is, the transverse buckling term in equation (3) is larger than the relaxation length γ_{11}. DeJuren and Swanson [5] also found imaginary diffusion lengths in graphite piles with sides less than 28 inches.

An important, additional consideration is the fact that the Grade HC graphite has many more impurities than the AGOT graphite normally

used in experiments of this nature. Mantell [17] lists the ash content for Grade HC as 0.30 per cent whereas for the AGOT graphite, the ash content is 0.07 per cent. Although no exact content breakdown listing was found for this particular grade, other manufacturers of graphite for similar applications list varying degrees of iron, vanadium, sulfur, calcium, titanium, aluminum and boron as constituents of ash. The presence of these elements could have a drastic effect upon reducing the diffusion length throughout the pile.

Appendix B discusses the uncertainty analysis and it is seen that very high inaccuracies are present for almost all data points, due to the low total count received and the relatively high background count. It should also be noted that the steepness of the thermal group slope makes it very sensitive to data variations.

VI. SUMMARY

It has been shown by theoretical analysis that the thermal diffusion length as illustrated by the relaxation length does, in fact, differ above and below the Bragg cut-off. Further, this difference decreases as temperature is increased, indicating that a single straight line (slope), or diffusion length, is approached throughout the entire thermal range at a sufficiently high temperature T_o, where T_o is greater than 1020°K. The slopes listed in Table 2 and shown in Figures 8 and 9 verify this analysis. Although the slopes thus obtained for the neutron group above the Bragg cut-off give lower than usual thermal group diffusion lengths, the trend is clearly brought out.

In the development of equation (2) we have assumed exponential decay and that the transverse leakage has no effect on the total flux spectrum. However, as shown by Williams [22], for crystalline moderators there is a maximum transverse buckling which invalidates this assumption. Theoretically, for the case of graphite, values of buckling for sides less than 45 inches will lead to a non-exponential decay of the flux, and its energy spectrum along the z direction will change. No discrete values of the relaxation length would exist in this case. DeJuren and Swanson [5] however reported a diffusion length measured in a graphite block with 28 inch sides. Only when their sizes were reduced to 20 inches did their diffusion lengths become imaginary. As DeJuren and Swanson showed in their experiments, the transverse leakage of neutrons increases along the z direction due to the fact that cold neutrons with longer mean free paths escape easier and therefore spectral equilibrium is not maintained.

This effect is apparent in the cold group region of figures 8 and 9. Due to the small size of the present pile, the spatial decay is no longer exponential and equation (2) can no longer be valid.

The heating capacity of this graphite pile has not been approached. Further work in this area at even higher temperatures should be done to verify this conclusion, which is based on only one high temperature test. It would be recommended however that provisions for a stronger neutron flux within the graphite be provided, in which case the thermal neutron sensitive dysprosium could still be used. The possibility should also be investigated of using a water cooled BF_3 detector in conjunction with a multi-channel analyzer. Either case will reduce the uncertainties presented here. Another important point is that the block size must be increased beyond the border line between the imaginary and real diffusion length regions. In fact, the size must be large enough to insure the existence of a diffusion length for the cold neutron group.

APPENDIX A FORMULAE FOR DATA REDUCTION

In determining the neutron flux, use is made of the radioactive atoms of dysprosium which are produced by neutron absorption within the wire detector. The rate of production R less the rate of decay A, called the activity, is equal to the rate of change of these radioactive atoms

$$\frac{dn}{dt} = R - \lambda n$$

where n is the number of radioactive atoms and λ is the decay constant. For steady flux cases R is a constant and the solution to the above equation can be written

$$A = \lambda n = A_s(1 - e^{-\lambda t}) \qquad (7)$$

where A_s, the saturation activity, is the equivalent of the rate of production R for very long irradiation times. After removal from irradiation the rate of decay will decrease exponentially as

$$A = \lambda n = A_j' e^{-\lambda t_i}$$

where t_i is the time after removal and A_j is the activity at removal time. If counting is employed to determine the number of radioactive atoms n existing over a given period of time, those counts C, less any background counts B, will be equal to the difference between the rate of decay at the beginning t_a and end t_b of counting time, divided by the decay constant and multiplied by the efficiency ε of the counting equipment.

$$n = C - B = \varepsilon \left[\frac{A_j}{\lambda} e^{-\lambda t_a} - \frac{A_j}{\lambda} e^{-\lambda t_b} \right]$$

$$\lambda(C - B) = \varepsilon A_j \left[e^{-\lambda t_a} - e^{-\lambda t_b} \right] \qquad (8)$$

In the case where the detector wire is alternately removed and inserted in a neutron flux, a recursive formula was derived for A_j. Referring to Figure 10, the initial activity at $t = 1$ will be simply

$$A_1 = A_s (1 - e^{-\lambda t_{i1}}) \qquad (9)$$

Between $t = 1$ and $t = 2$, the value of A_1 will decrease an amount $A_1 e^{-\lambda t_{o2}}$. Thus the value of X will equal

$$X = A_1 e^{-\lambda t_{o2}} \qquad (10)$$

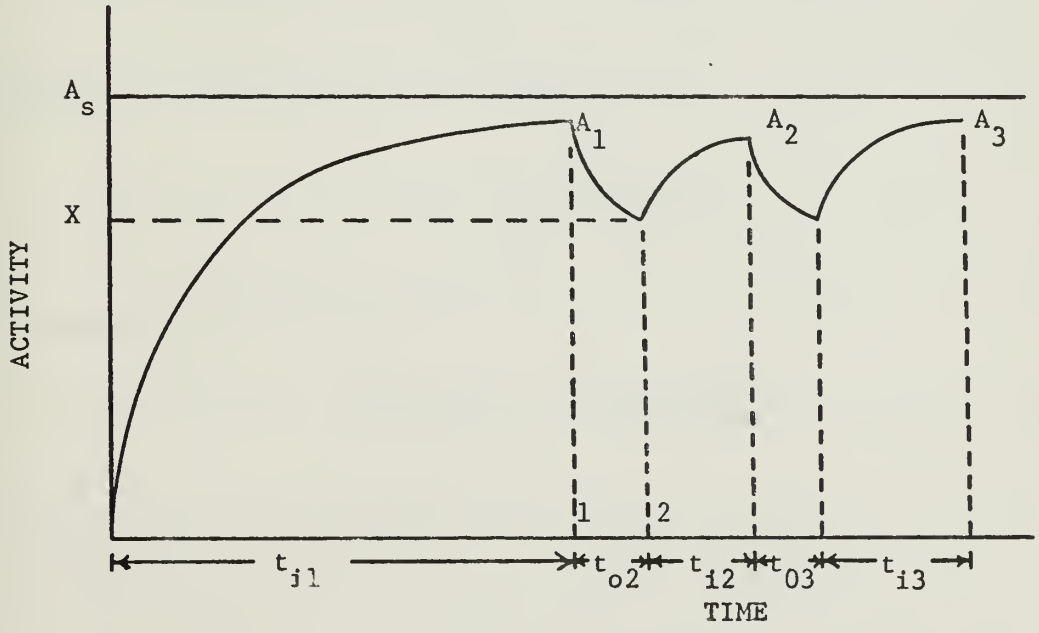

Fig. 10

Repeated Exposure and Withdrawal From Flux

Considering an exponential rise again at point X and time starting over at $t = 2$, the value of A_2 is

$$A_2 = X + (A_s - X)(1 - e^{-\lambda t_{i2}})$$

$$A_2 = X\, e^{-\lambda t_{i2}} + A_s (1 - e^{-\lambda t_{i2}}) \qquad (11)$$

Combining equations (10) and (11)

$$A_2 = A_1\, e^{-\lambda(t_{o2}+t_{i2})} + A_s (1 - e^{-\lambda t_{i2}})$$

and from equation (9)

$$A_2 = A_s(1 - e^{-\lambda t_{i1}})\, e^{-\lambda(t_{o2}+t_{i2})} + A_s(1 - e^{-\lambda t_{i2}})$$

which can be written

$$A_2 = A_s \left[1 - e^{-\lambda t_{i2}} + (1 - e^{-\lambda t_{i1}})e^{-\lambda(t_{o2}+t_{i2})} \right]$$

A similar line of reasoning can be applied to A_3

$$A_3 = A_s \left[1 - e^{-\lambda t_{i3}} + A_2\, e^{-\lambda(t_{o3}+t_{i3})} \right]$$

the recursive formula being

$$A_j = A_s \left[1 - e^{-\lambda t_{ij}} + A_{j-1}\, e^{-\lambda(t_{oj}+t_{ij})} \right] \quad , j=2,3,... \qquad (12)$$

Equation (9) is still valid for $j = 1$. From equations (8) and (12)

$$A_s = \frac{\lambda(C - B)}{\varepsilon \left[- e^{-\lambda t_{ij}} + A_{j-1}\, e^{-\lambda(t_{oj}+t_{ij})} \right] (e^{-\lambda t_a} - e^{-\lambda t_b})} \qquad (13)$$

For the case where the flux is constant the saturated activity can be written

$$A_s = N_T \int \sigma_a(E)\phi(E)\, dE$$

where N_T is the total number of target neutrons and $\sigma_a(E)$ is the capture cross section at energy E. Since the dysprosium was within two per cent of indicating only thermal energy neutrons, the integration can be carried out over the thermal energy range. Considering a Maxwellian flux and assuming a 1/v behavior for dysprosium, the saturation activity can be written

$$A_s = N_T \sigma_a \phi \left(\frac{\pi T_o}{4T} \right)^{1/2} \qquad (14)$$

where T_o is 293.16°K, T is the medium temperature, and σ_a = 920 b. is the capture cross section recommended in Ref. 7. It is based on the weighted cross sections for Dy isotopes by their abundance in natural dysprosium. Equations (13) and (14) now give, for the thermal neutron flux

$$\phi = \frac{\lambda(C - B)}{\varepsilon A_j \left(e^{-\lambda t_a} - e^{-\lambda t_b} \right) \sigma_a \left(\frac{\pi T_o}{4T} \right)^{1/2} N_T} \qquad (15)$$

N_T, the total number of target neutrons, can be found by

$$N_T = V \left(\frac{WT/V \cdot A_o}{A} \right) \nu$$

where V is the wire volume, WT is the wire weight, A_o is Avogadro's number, A is the average atomic mass, and ν is the fraction by weight of dysprosium in the Dy-Al wire.

APPENDIX B UNCERTAINTY ANALYSIS

As stated earlier the low thermal flux resulted in a relatively low count rate compared to the background count. An analysis was conducted on each of the data points to determine the accuracy of the resulting flux.

Considering a total of C counts as the mean value, its standard deviation can be written as $C^{1/2}$, and the total count would be reported as $C \pm C^{1/2}$. The same criterion is applied to the background count B. In obtaining the difference, C - B, over the same time interval, the value with its standard deviation is

$$(C - B) \pm (\sigma_C^2 + \sigma_B^2)^{1/2}$$

where the standard deviations are

$$\sigma_C = C^{1/2} \qquad \text{and}$$

$$\sigma_B = B^{1/2}$$

This value is converted into a percentage error by

$$(C - B) \pm \frac{(\sigma_C^2 + \sigma_B^2)^{1/2}}{(C - B)} \quad 100\%$$

Since this was the major source of uncertainty in determining the flux, the same percentage error applies to the thermal flux obtained for each data point. These uncertainties in terms of percentage are tabulated in Tables 3 and 4 at the end of the Appendix.

When the data points were plotted there were some obviously erratic points. It seemed appropriate to disregard some of the more erroneous

ones. Therefore a least squares approximation, based on equation (6), was obtained on the computer. The standard deviation of the total of all data points was also obtained from the best fit straight line. Using Chevenet's criterion for rejection of outlying data, a ratio $(\frac{d_i}{\sigma})$ of data deviation from its mean value to the standard deviation was obtained for each position. Those points giving ratios outside the criterion were rejected and those less than the criterion were resubmitted for a second least squares approximation. It is this second approximation for slope that is used for the final results and discussion. The ratios obtained as above are also listed in Tables 3 and 4.

The high temperature uncertainty was determined as follows, utilizing the voltage readings in all calculations. When the final value was obtained, the conversion to degrees centigrade was applied. At each of the levels, upper and lower,

$$\bar{v} = \frac{1}{N} \sum_{i=1}^{N} v_i$$

$$\sigma = \left[\frac{1}{N-1} \sum_{i=1}^{N} (\bar{v} - v_i)^2 \right]^{1/2}$$

where v_i are each of the five thermocouple readings at one recording time and N is equal to the number of thermocouples. Then the mean and deviation for the pile at each recording instance is found

$$\bar{v} = \frac{1}{2} (\bar{v}_u + \bar{v}_\ell)$$

$$\sigma_v = \frac{1}{2} (\sigma_u^2 + \sigma_\ell^2)^{1/2}$$

where the subscripts u and ℓ refer to upper and lower levels,

respectively. The overall temperature value and its standard deviation is then obtained from the mean values of each recorded run:

$$\bar{v}_m = \frac{1}{N} \sum_{i=1}^{N} \bar{v}_i$$

$$\sigma_m = \left[\sum_{i=1}^{N} \sigma_{v_i}^2 \right]^{1/2}$$

Using the above procedure a high temperature of 207.88 ± 4.56°C was obtained.

TABLE 3

Temperature: 295°K

Height above base (cm)	Flux (n/cm^2sec)	Error (per cent)	$\frac{d_i}{\sigma}$	Chevenet's Criterion
35.21	2354.8	8.60	0.05	1.73
37.65	1926.5	11.61	0.57	1.73
40.11	1686.2	11.25	0.14	1.73
42.57	1311.7	17.30	1.25	1.73
45.02	1523.3	12.62	4.51	1.73
47.53	849.6	25.35	2.79	1.73
49.99	896.9	20.25	2.93	2.13
52.43	978.9	21.30	0.14	2.13
54.85	761.4	22.75	4.12	2.13
57.29	798.4	24.95	1.23	2.13
59.75	692.7	21.85	1.64	2.13
62.21	752.9	23.50	0.69	2.13
64.63	557.5	27.20	3.19	2.13
67.03	523.9	32.90	3.52	2.13
69.47	492.4	30.90	3.69	2.13
71.91	748.2	24.30	3.82	2.13
74.35	436.3	34.70	9.26	2.13
76.81	563.1	31.50	4.01	2.13
79.25	439.8	35.20	4.59	2.13
81.67	389.9	45.90	0.64	2.13

TABLE 4

Temperature: 481°K

Height above base (cm)	Flux (n/cm^2sec)	Error (per cent)	$\frac{d_i}{\sigma}$	Chevenet's Criterion
32.75	5518.9	10.35	0.32	1.90
35.21	8612.5	13.55	4.93	1.90
37.65	2204.9	20.23	3.48	1.90
50.11	1713.0	12.17	3.87	1.90
42.57	2169.6	12.17	0.78	1.90
45.02	2502.8	15.74	1.66	1.90
47.53	1671.0	19.00	0.19	1.90
49.99	1547.5	24.40	1.04	1.90
52.43	1204.2	30.50	1.76	2.10
54.85	3291.3	31.55	3.01	2.10
57.29	890.6	30.90	7.79	2.10
59.75	1055.6	26.50	3.59	2.10
62.21	1050.0	39.75	0.79	2.10
64.63	802.9	36.30	0.32	2.10
67.03	740.4	30.45	1.11	2.10
69.47	1022.5	32.10	0.74	2.10
71.91	828.8	152.50	3.52	2.10
74.35	646.8	115.00	2.59	2.10
76.81	222.1	149.50	1.43	2.10
79.25	466.9	54.90	6.50	2.10
81.67	(neg)	74.70	1.79	2.10

BIBLIOGRAPHY

1. Ahmed, F., Journal of Nuclear Energy Parts A/B, v. 19, (1965), p. 703-705.

2. Ahmed, F., Nuclear Science and Engineering, v. 23, (1965), p. 203-205.

3. Beckurts, K. H. and Wirtz, K., Neutron Physics, p. 30, Springer-Verlag, 1964.

4. Ben-David, G. and Huebschmann, B., Journal of Nuclear Energy Parts A/B, v. 16, (1962), p. 291-295.

5. DeJuren, J. A. and Swanson, V. A., Journal of Nuclear Energy Parts A/B, v. 20, (1966), p. 905-914.

6. Egelstaff, P. A., Journal of Nuclear Energy, v. 5, (1957), p. 203-209.

7. Goldberg, M. D., and others, Neutron Cross Sections, 2nd Edition Supplement 2 to BNL 325, Volume IIC, U. S. Atomic Energy Commission Document, Associated Universities, 1966.

8. Guy, A. G., Elements of Physical Metallurgy, p. 90-91, 103, Addison, Wesley Publishing Company, 1959.

9. Holman, J. P., Experimental Methods for Engineers, p. 53, McGraw-Hill, 1966.

10. Hughes, D. J., Pile Neutron Research, Addison-Wesley Publishing Company, 1953.

11. Hughes, D. J. and Schwartz, R. B., Neutron Cross Sections, 2nd Edition, p. 95, U. S. Atomic Energy Commission Document BNL 325, Associated Universities, 1958.

12. Kaiser, R. E., and Kimel, W. R., Nuclear Science and Engineering, v. 20, (1964), p. 468-475.

13. Kothari, L. S., and Khubchandani, P. G., Nuclear Science and Engineering, v. 7, (1960), p. 240-244.

14. Kruger, P., Nucleonics, v. 17, (1959), p. 116.

15. Lamarsh, J. R., Introduction to Nuclear Reactor Theory, Addison-Wesley Publishing Co., 1966.

16. Lloyd, R. C., Clayton, E. D., and Richey, C. R., Nuclear Science and Engineering, v. 4, (1958), p. 690-697.

17. Mantell, C. L., Carbon and Graphite Handbook, John Wiley & Sons, 1968.

18. Ross, C. W., Effect of Thermal Neutron Irradiation on Thermocouples and Resistance Thermometers, paper presented at Joint Nuclear Instrumentation Symposium, Raleigh, N. C., September 8, 1961.

19. Scoville, J. J., Fast, E., and Rogers, J. W., Nuclear Science and Engineering, v. 25-1, (1966), p. 12.

20. Tittle, C. W., Nucleonics, v. 9, (1951), p. 60.

21. Trikha, S. K., and others, Journal of Nuclear Energy, v. 21, (1967), p. 819.

22. Williams, M. M. R., On the existence of a Diffusion Length in a Finite Prism of Pure Moderator, paper presented at International Atomic Energy Agency Symposium on Neutron Thermalization and Reactor Spectra, Ann Arbor, Michigan, 17-21 July 1967.

INITIAL DISTRIBUTION LIST

		No. Copies
1.	Defense Documentation Center Cameron Station Alexandria, Virginia 22314	2
2.	Library, Code 0212 Naval Postgraduate School Monterey, California 93940	2
3.	Professor D. H. Nguyen, Code 59Ng Department of Mechanical Engineering Naval Postgraduate School Monterey, California 93940	1
4.	LCDR Frederick F. Touchstone, Jr., USN 12 Melrob Court, Apt. 1 Annapolis, Maryland 21403	1

Security Classification

DOCUMENT CONTROL DATA - R & D

(Security classification of title, body of abstract and indexing annotation must be entered when the overall report is classified)

1. ORIGINATING ACTIVITY (Corporate author)	2a. REPORT SECURITY CLASSIFICATION
Naval Postgraduate School Monterey, California 93940	Unclassified
	2b. GROUP

3. REPORT TITLE

The Temperature Dependence of Thermal Neutron Diffusion Length in Graphite

4. DESCRIPTIVE NOTES (Type of report and inclusive dates)

Master's Thesis; June 1970

5. AUTHOR(S) (First name, middle initial, last name)

Frederick Faber Touchstone, Jr.

6. REPORT DATE	7a. TOTAL NO. OF PAGES	7b. NO. OF REFS
June 1970	54	22

8a. CONTRACT OR GRANT NO.	9a. ORIGINATOR'S REPORT NUMBER(S)
b. PROJECT NO.	
c.	9b. OTHER REPORT NO(S) (Any other numbers that may be assigned this report)
d.	

10. DISTRIBUTION STATEMENT

This document has been approved for public release and sale; its distribution is unlimited.

11. SUPPLEMENTARY NOTES	12. SPONSORING MILITARY ACTIVITY
	Naval Postgraduate School Monterey, California 93940

13. ABSTRACT

The existence of the two classes of thermal neutrons about the Bragg cut-off in a crystalline structure has been experimentally verified by the use of dysprosium-aluminum wire detector. The space dependent neutron flux in a 24x24x48 inch rectangular parallelopiped graphite pile, GLC grade HC and density 1.60 gm/cm^3, has been investigated at 295°K and 481°K. At each temperature a distinct "knuckle" or change of neutron distribution is readily apparent, although this degree of change decreases with increasing temperature because the neutron cross section below the Bragg cut-off increases with increasing temperature.

DD FORM 1 NOV 65 1473 (PAGE 1)

S/N 0101-807-6811

Security Classification

A-31408

KEY WORDS	LINK A		LINK B		LINK C	
	ROLE	WT	ROLE	WT	ROLE	WT
thermal neutrons in graphite						
Bragg cut-off effect in graphite						
diffusion length in graphite						

Thesis
T7624
c.1

120008

Touchstone
The temperature dependence of thermal neutron diffusion length in graphite.

Thesis
T7624
c.1

120008

Touchstone
The temperature dependence of thermal neutron diffusion length in graphite.

3 2 '68 002 03605 5
LIBRARY